One-Pot Combustion Synthesis of Nickel Oxide and Hematite: from Simple Coordination Compounds to High Purity Metal Oxide Nanoparticles

Dejan Jeremić[1], Ljubica Andjelković[2], Milica R. Milenković[3], Marija Šuljagić[2], Maja Šumar Ristović[3], Sanja Ostojić[4], Aleksandar S. Nikolić[3], Predrag Vulić[5], Ilija Brčeski[3*], Vladimir Pavlović[6,7]

[1]Innovation Center of the Faculty of Chemistry, University of Belgrade, Studentski Trg 12-16, 11000 Belgrade, Serbia

[2]University of Belgrade, Institute of Chemistry, Technology and Metallurgy, Department of Chemistry, Njegoševa 12, 11000, Belgrade, Serbia

[3]Faculty of Chemistry, University of Belgrade, Studentski Trg 12-16, 11000 Belgrade, Serbia

[4]Institute of General and Physical Chemistry – IOFH, Studentski Trg 12/V, Belgrade, 11000, Serbia

[5]Faculty of Mining and Geology, University of Belgrade, Djušina 7, 11000 Belgrade, Serbia

[6]Faculty of Agriculture, University of Belgrade, Belgrade, 11000, Serbia

[7]Institute of Technical Sciences of SASA, Knez Mihailova 35/IV, Belgrade, 11000, Serbia

Abstract:

This work is the first report of a very simple and fast one-pot synthesis of nickel oxide (NiO) and hematite (α-Fe_2O_3) nanoparticles by thermal decomposition of transition metal aqua complexes with camphor sulfonate anions. Obtained nanopowders were characterized by X-ray powder diffraction, Fourier transform IR analysis, scanning electron microscopy, and Energy-dispersive X-ray spectroscopy. X-ray powder diffraction confirmed the formation of high purity NiO and α-Fe_2O_3 crystal phases. In the case of α-Fe_2O_3, about five times larger average crystallite size was obtained. Fourier transform IR spectra of synthesized materials showed characteristic peaks for NiO and α-Fe_2O_3 nanostructures. To visualize the morphology and the chemical composition of the final products Scanning electron microscopy and Energy-dispersive X-ray spectroscopy were performed. The thermogravimetric analysis was done for a better understanding of the general thermal behavior of precursor compounds. This easy-to-perform and fast preparation method opens a broad range of obtained materials' usage, particularly due to its economic viability.

Keywords: *Nanomaterials; Nickel oxide; Hematite; camphor sulfonates; One-pot synthesis.*

1. Introduction

There is a continuous scientific demand for cheap, simple, environmentally sound and economically sustainable routes to develop, design and produce advanced functional

_____

*⁎) **Corresponding author:** ibrceski@chem.bg.ac.rs

_____

nanomaterials. The modern technologies particularly require faster development of metal oxide materials at the nanometric level, striving for cheaper precursors and new synthesis methods of nanostructures with uniform physico-chemical properties [1-4].

Oxide nanomaterials based on iron and nickel have no competitors for their electrochemical, adsorption, sensing and/or catalytic performances, as their high specific surface areas lead to rich contact between the active materials and the electrolyte/pollutants [5-19].

This type of materials can exhibit various size-, shape-, and morphology-dependent properties by a slight change in the preparation procedure [12, 20-24]. Sintering appeared to be one of the best processes for obtaining oxide materials and improving their physical and chemical properties [25-30]. Although many synthetic approaches were developed [31-39], emphasis should be pointed out to thermal decomposition of suitable precursors for the preparation of functional oxide nanomaterials with tailored properties at mass scale [40]. Coordination compounds, such as metal carbonyls, metal acetylacetonates, and metal carboxylates, have been profoundly investigated as precursors to fabricate nanostructured metal oxides with desired morphology by thermal decomposition [40-47]. Organic solvents are widely used in thermal decomposition methods, to lower reaction temperatures and provide uniform and narrow size distribution of nanoparticles [40, 48]. However, extensive use of such solvents is environmentally inexcusable. Stable, large single crystals of isomorphous hexaaquametal(II) D-camphor-10-sulfonate might be potentially used as optical filters and optical materials [49]. Despite their applications in optics, such compounds can be recognized as precursors for the synthesis of oxide nanomaterials by thermal decomposition, due to their high purity and easy, fast, and cheap production. It is expected that the presence of organic anion in these compounds can enable the avoidance of additional organic solvents in one-pot combustion syntheses, opening the way to an eco-friendly preparation method for metal oxides. To the best of our knowledge, hexaaquametal(II) D-camphor-10-sulfonates have not been investigated in this manner.

Having all this in a mind, in this paper, an alternative approach for producing nano-sized nickel oxide (NiO) and hematite (α-Fe_2O_3) powders at low cost by thermal decomposition of appropriate camphor sulfonate precursors is presented.

2. Materials and Experimental Procedures

Synthesis procedures and crystal structure analyses of hexaaquanickel(II) D-camphor-10-sulfonate i.e. $[Ni(H_2O)_6](CSA)_2$ and hexaaquairon(II) D-camphor-10-sulfonate i.e. $[Fe(H_2O)_6](CSA)_2$ (where CSA is D-camphor-10-sulfonate) have been previously reported [49,50]. In this work previously reported synthetic procedure for $[Ni(H_2O)_6](CSA)_2$ was slightly modified, i.e. basic nickel carbonate was used instead of nickel bromide.

Briefly, D-camphor-10-sulfonic acid solution (35.0 g, 0.15 mol) in deionized water (60 mL) was added to basic nickel carbonate (21.4 g, 0.18 mol). The reaction mixture was refluxed for 48 h followed by filtration. After cooling in a refrigerator (2 weeks) crystals of hexaaquanickel(II) D-camphor-10-sulfonate were obtained (yield 63 %, 29.73 g).

D-Camphor-10-sulfonic acid monohydrate (35.0 g, 0.15 mol) was dissolved in deionized water (60 mL). Iron chips (10.0 g, 0.18 mol) were added in D-camphor-10-sulfonic acid solution. Than the reaction mixture was refluxed for 48 h and filtered off. The solution has been cool down in a refrigerator until the orange crystals of hexaaquairon(II) D-camphor-10-sulfonate were obtained (yield 68 %, 31.95 g).

NiO and α-Fe_2O_3 were synthesized by thermal decomposition of the solid camphor sulfonate precursors (5 g), in an electrical furnace with a heating rate of 10 °C/min at $T = 550$ °C for 3 hours, followed by pulverization in an agate mortar.

X-ray powder diffraction (XRPD) patterns for the final products of thermal degradation were collected using a Rigaku SmartLab automated powder X-ray diffractometer with Cu Kα1,2 ($\lambda = 1.54059$ Å) radiation (U = 40 kV, I = 30 mA) equipped with D/teX Ultra 250 stripped 1D detector in the XRF reduction mode. The diffraction angle range was 20–120° 2θ with a step of 0.01° at a scan speed of 2°/min. The structural and microstructural investigation of the final products after thermal decomposition was conducted by the Rietveld method.

The IR spectra were recorded on a Nicolet 6700 FT-IR instrument (Thermo Scientific), in the ranges of 4000–400 and 700–240 cm^{-1} using the ATR technique with a Smart Orbit accessory (diamond crystal).

Scanning electron microscopy (SEM) and Energy-dispersive X-ray spectroscopy (EDS) analyses of the final products were performed with a JEOL JSM-6390LV scanning electron microscope. EDS analyses were conducted in the area of 1×10^4 μm^2 per sample.

A thermogravimetric analysis (TGA) of $[Ni(H_2O)_6](CSA)_2$ and $[Fe(H_2O)_6](CSA)_2$ was performed by Thermogravimetric Analyser TGA Q500 (TA Instruments, New Castle, DE USA). The samples' weights were 10.6080 and 10.6820 mg for $[Ni(H_2O)_6](CSA)_2$ and $[Fe(H_2O)_6](CSA)_2$, respectively. All TGA experiments were conducted in O_2 as the purge gas, with purge flow 50 mL/min. While the heating rate was 10 °C/min, the applied temperature was ranging from 25 to 800 °C. For all experiments, the Pt crucibles were used.

3. Results and Discussion

Thermal decomposition of hexaaquametal(II) D-camphor-10-sulfonates was performed at 550 °C in electrical furnace, without the addition of any organic compound. The obtained powders were characterized by XRPD, IR spectroscopy, SEM and EDS analyses. In the aim to better understand the degradation processes of precursors, TG and DTG analyses are performed.

XRPD was performed to identify the composition and crystalline phase of the final products. The obtained XRPD results were analyzed by the Rietveld method to gain deeper insight into the structural and microstructural parameters, by the fundamental parameters approach [51], as implemented in PDXL2 Rigaku software.

Fig. 1 shows the XRPD patterns of the face-centered cubic phase of NiO (ICDD PDF 47-1049) and the rhombohedral structure of α-Fe$_2$O$_3$ (ICDD PDF 33-0664), respectively. No other diffraction peaks corresponding to impurities were observed. The X-ray diffraction patterns show broad peaks indicating the ultrafine nature and small crystallite size of the particles.

Tab. I Unit cell parameters (Å), volumes (Å^3) and microstructural parameters for the final powders obtained by thermal decomposition of $[Ni(H_2O)_6](CSA)_2$ and $[Fe(H_2O)_6](CSA)_2$.

Crystal phase	NiO	α-Fe$_2$O$_3$
Space group	$Fm\overline{3}m$	$R\overline{3}c$
Unit cell parameter, a (Å)	4.1774(1)	5.03395(6)
Unit cell parameter, c (Å)	---	13.7495(3)
V (Å^3)	72.899(4)	603.485(4)
Crystallite Size (nm)	10.8(1)	58.5(4)
Microstrain (%)	0.099(6)	0.041(3)

_____

The values of average crystallite size and microstrain obtained by the Rietveld methods are listed in Table I. An average crystallite size in NiO was 10.8(1) nm, while approximately 5 times larger average crystallite size was observed for α-Fe_2O_3. This result can be explained by a higher rate of crystal growth in the rhombohedral crystal structure of α-Fe_2O_3 than in the face-centered cubic crystal lattice of NiO. It is a consequence of lower energy (i.e. lower temperature) necessary for the growth of α-Fe_2O_3 phase than in the case of crystal growth of NiO phase. However, the preparation of single-phase nanocrystalline metal oxides by thermal decomposition of solid camphor sulfonate precursors at relatively low temperatures without using additional organic compounds should not be neglected.
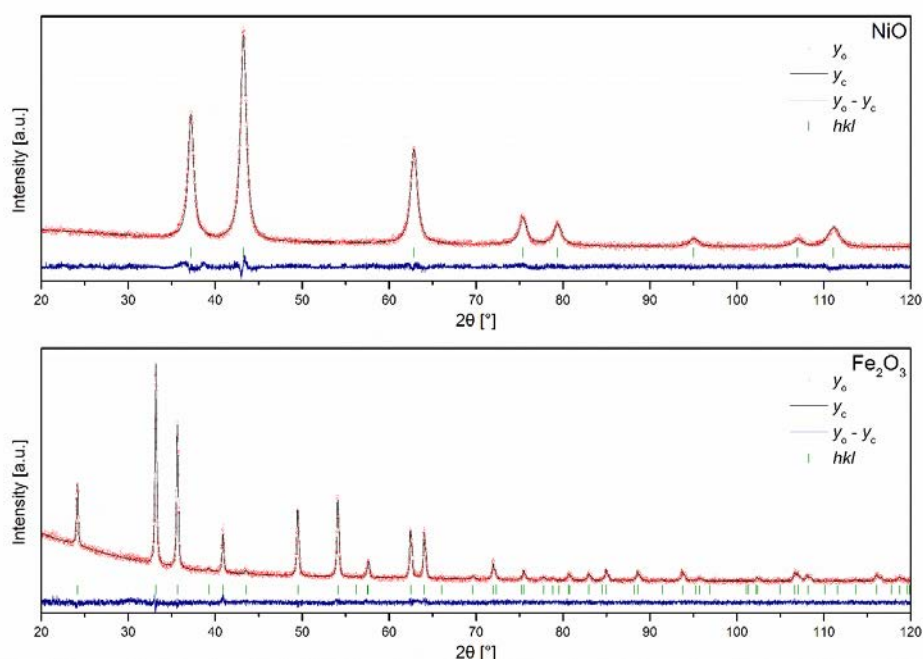

Fig. 1. XRPD patterns of final powders obtained by thermal decomposition of $[Ni(H_2O)_6](CSA)_2$ and $[Fe(H_2O)_6](CSA)_2$.

The vibration modes are strongly influenced by the crystallite sizes. Thereby, the IR spectrum is a fingerprint of nanocrystalline structure. The IR spectroscopy results confirmed the formation of nanocrystalline NiO and α-Fe_2O_3. The IR spectrum of NiO shows a characteristic peak at 457 cm^{-1}, Fig. 2, assigned to Ni−O stretching vibration as was reported earlier by other researchers [34, 52]. The IR spectrum of α-Fe_2O_3 shows two characteristic bands at 441 and 521 cm^{-1} of the Fe–O bond, resulting from the tetrahedral and octahedral sites of hematite, respectively [53,54]. A broad peak approximately 3300 cm^{-1} (~3400 cm^{-1} in the IR spectrum of hematite) arises due to the presence of water, Fig. 2. A band observed about 1650 cm^{-1} in the spectra of both investigated samples can be attributed to the bending vibration of water.

IR spectra of camphor sulfonate precursors contain a strong band at 3416 cm^{-1} belonging to coordinated water molecules. Furthermore, two very strong bands at 1168 and 1045 cm^{-1}, corresponding to –SO_3 group of camphor sulfonate anion, are present. The bands assigned to the vibrations of the aliphatic alkyl groups at about 2950 cm^{-1}, as well as the band of the carbonyl group at 1734 cm^{-1} originate from camphor sulfonate moiety [49].

In summary, in the samples obtained by thermal decomposition of appropriate camphor sulfonate precursors, bands characteristic for camphor sulfonate anion are not detected in IR spectra, Fig. 2.
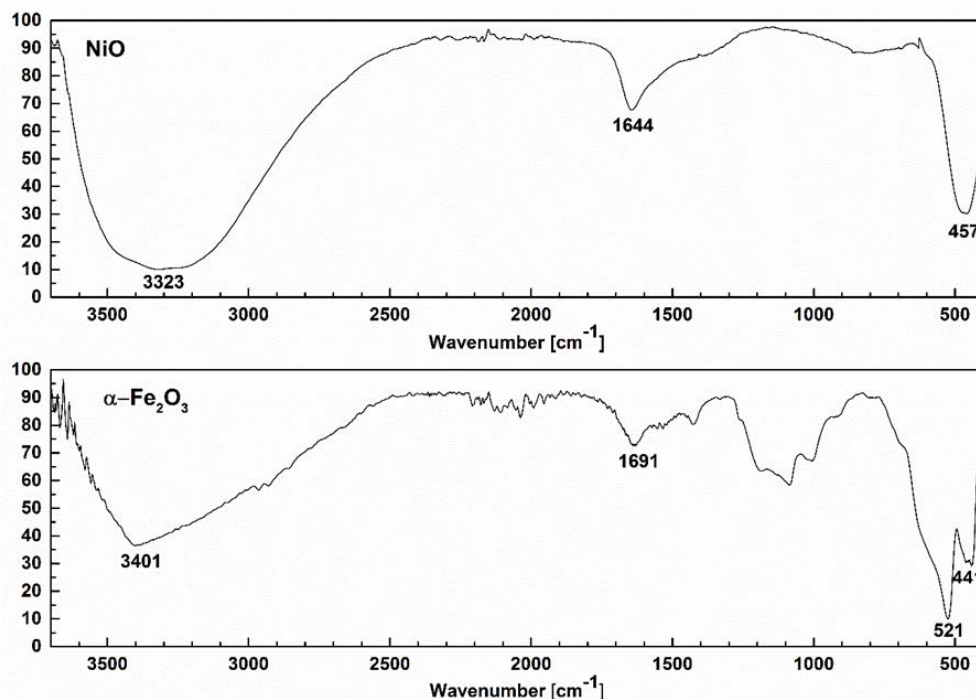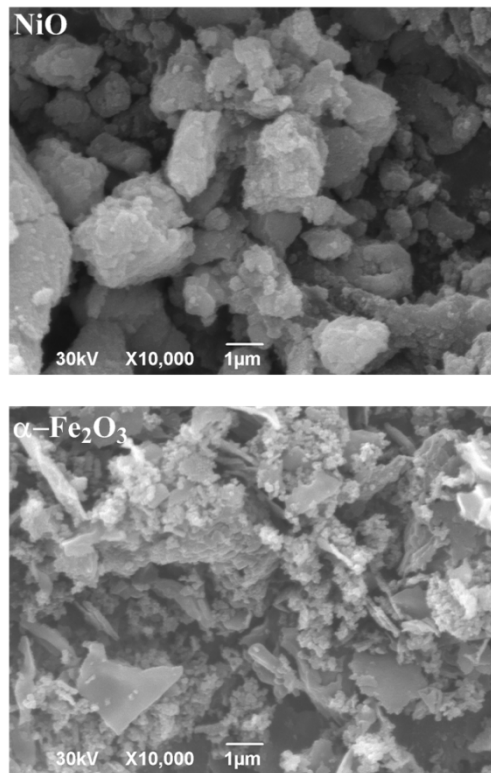
Fig. 2. FT-IR spectra of NiO and α-Fe$_2$O$_3$ powders obtained by thermal decomposition of appropriate camphor sulfonate precursors.

Bearing in mind that the nanocrystalline form of metal oxides strongly affects material microstructure, SEM and EDS analyses were performed to visualize the morphology and the chemical composition of the final products obtained by thermal decomposition of appropriate camphor sulfonate precursors. From the obtained SEM results, Fig. 3, it was clear that the obtained powders were highly agglomerated, as a consequence of their nanometric sizes. NiO sample is consisted of spherically shaped agglomerates, while in α-Fe$_2$O$_3$ powder two forms of aggregates, spherical and plate-like, are observed. The EDS spectrum of NiO powder shows only Ni and O, indicating that material with high degree of purity was obtained, Fig. 4. A similar atomic percentage of Ni and O were observed by EDS analysis of NiO, Table II. In the case of α-Fe$_2$O$_3$, only Fe and O are present in the EDS spectrum, Fig. 4. Furthermore, EDS analysis revealed the exact stoichiometric ratio of 2:3 was obtained, Table II.

Tab. II Weight and atomic percentage of elements in NiO and α-Fe$_2$O$_3$ samples obtained by EDS analyses.

Element	NiO		α-Fe$_2$O$_3$	
	Wt %	Atomic %	Wt %	Atomic %
Ni	75.09	46.66	---	---
Fe	---	---	69.44	39.43
O	24.91	53.34	30.56	60.57
Total	100.00	100.00	100.00	100.00

_____

Fig. 3. SEM analysis of NiO and α-Fe$_2$O$_3$ powders obtained by thermal decomposition of appropriate camphor sulfonate precursors.
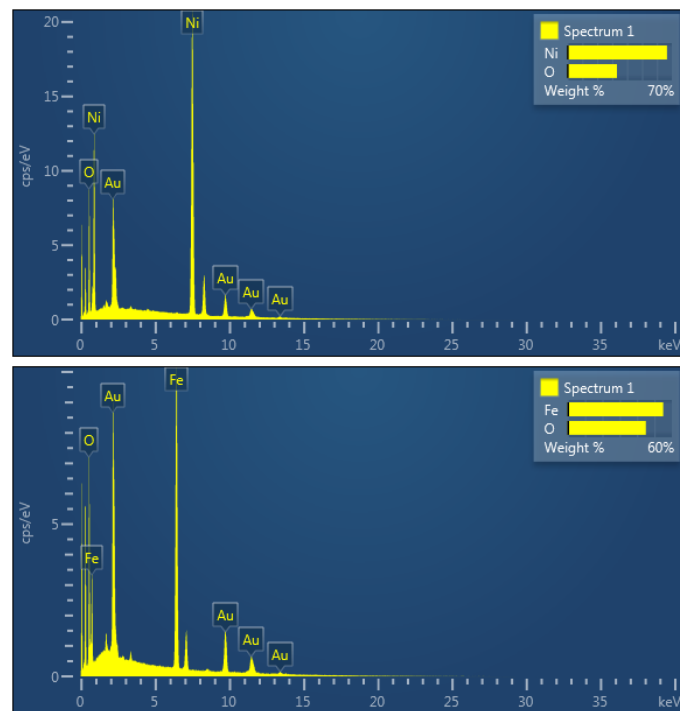
Fig. 4. EDS spectra of NiO and α-Fe$_2$O$_3$ powders.

The TG and DTG curves of $[Ni(H_2O)_6](CSA)_2$ and $[Fe(H_2O)_6](CSA)_2$ are shown in Fig. 5. General thermal behavior of these compounds, i.e. stability ranges and mass loss data are listed in Table III.

The degradation of $[Ni(H_2O)_6](CSA)_2$ and $[Fe(H_2O)_6](CSA)_2$ in O_2 atmosphere occurs in two main steps. Thermal analysis showed that the multi-step degradation of both compounds begins at about 50 ^{o}C with the loss of six molecules of coordinated water. Degradation continues in temperature range 282-532 ^{o}C for $[Ni(H_2O)_6](CSA)_2$, and 203-440 ^{o}C for $[Fe(H_2O)_6](CSA)_2$. The second degradation step for both compounds contains several successive degradation steps overlapped in this temperature range. However, this step can be ascribed to the combustion of the organic groups-products of CSAs. In the case of $[Fe(H_2O)_6](CSA)_2$, Fe(II) has been oxidized to Fe(III) in the temperature range from 404-440 ^{o}C. Degradation residue of Ni(II) compound at 532 ^{o}C corresponds to black NiO, whilst final residue of $[Fe(H_2O)_6](CSA)_2$ degradation at 440 ^{o}C is red Fe_2O_3.
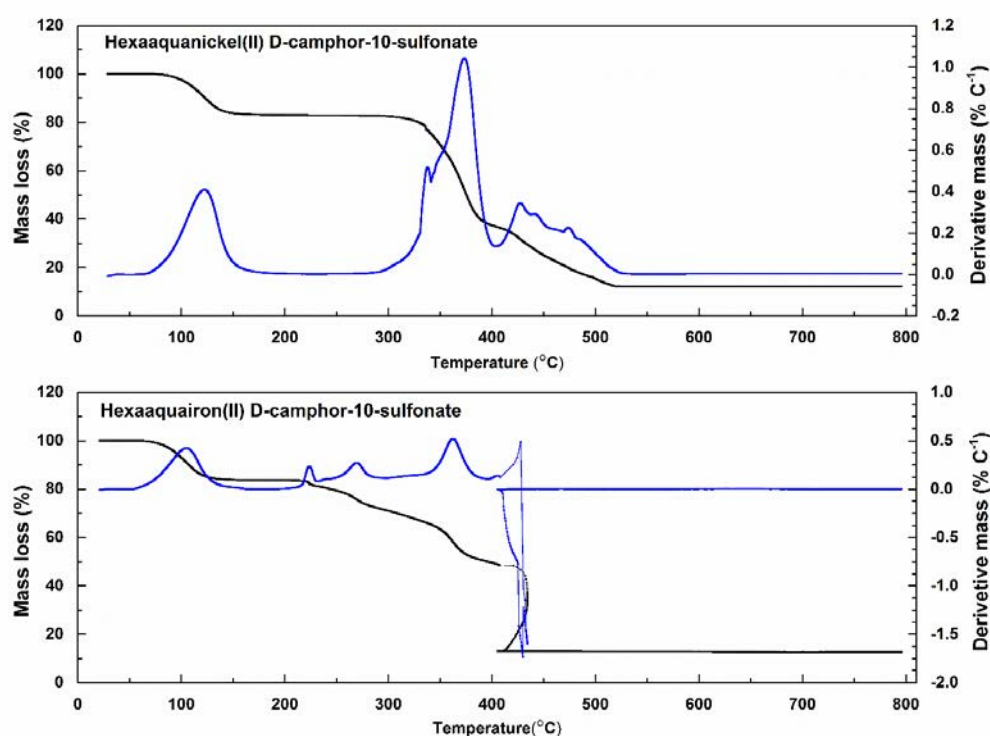
Fig. 5. TG and DTG curves of $[Ni(H_2O)_6](CSA)_2$ (up) and $[Fe(H_2O)_6](CSA)_2$ (down).

Tab. III Decomposition temperature ranges and mass loss data for $[Ni(H_2O)_6](CSA)_2$ and $[Fe(H_2O)_6](CSA)_2$.

Compound	Decomposition temperature range (^{o}C)	Mass loss found / %	Mass loss calculated / %	Fragment loss
$[Ni(H_2O)_6](CSA)_2$	58–178	107.80/17.13	108.06/17.17	6 H_2O
	282–532	445.69/70.82	446.07/70.88	degradation products of CSAs
$[Fe(H_2O)_6](CSA)_2$	52–152	101.99/16.28	108.06/17.25	6 H_2O
	203–440	441.73/70.51	438.59/70.01	degradation products of CSAs

_____

4. Conclusion

The one-pot combustion syntheses of NiO and α-Fe$_2$O$_3$ powders at a nanoscale level were conducted by thermal decomposition of appropriate hexaaquametal(II) D-camphor-10-sulfonate precursors since the chemical composition of these compounds allows the avoidance of additional organic solvents. Furthermore, here described a new method for preparation of NiO and α-Fe$_2$O$_3$ was fully optimized at relatively low temperatures in a short time and using inexpensive, carefully chosen, precursors. The obtained metal oxide nanopowders are of high purity. Their microstructure indicates that such materials can be highly exploited. Therefore, the further step of our investigations will encompass the study on their electrochemical, sensing, and/or catalytic performances.

Acknowledgments

5. References

1. M. Chavali, M. Nikolova, SN Appl. Sci., 1 (2019) 607.
2. S. A. Corr, Metal oxide nanoparticles, in: Nanosci. Vol. 1 Nanostructures through Chem., The Royal Society of Chemistry, 2013: 180-207.
3. G. R. Patzke, Y. Zhou, R. Kontic, F. Conrad, Angew. Chemie Int. Ed., 50 (2011) 826.
4. C. N. R. Rao, H. S. S. Ramakrishna Matte, R. Voggu, A. Govindaraj, Dalt. Trans., 41 (2012) 5089.
5. W. Xiang, W.-Y. Liu, J. Zhang, S. Wang, T.-T. Zhang, K. Yin, X. Peng, Y.-C. Jiang, K.-H. Liu, X.-D. Guo, J. Alloys Compd., 775 (2019) 72.
6. D. Wu, W. Zhao, H. Wu, Z. Chen, H. Li, L.Y. Zhang, Scr. Mater., 178 (2020) 187.
7. B. H. R. Suryanto, Y. Wang, R. K. Hocking, W. Adamson, C. Zhao, Nat. Commun., 10 (2019) 5599.
8. Y. Liu, C. Gao, Q. Li, H. Pang, Chem. – A Eur. J. 25 (2019) 2141.
9. S. Kim, W.S. Yang, H.-J. Kim, H.-N. Lee, T.J. Park, S.-J. Seo, Y.M. Park, Ceram. Int., 45 (2019) 23370.
10. F. Yang, H. Su, Y. Zhu, J. Chen, W.M. Lau, D. Zhang, Scr. Mater., 68 (2013) 873.
11. W. Zhou, L. Guo, Chem. Soc. Rev., 44 (2015) 6697.
12. Z. Cao, M. Qin, B. Jia, Y. Gu, P. Chen, A.A. Volinsky, X. Qu, Ceram. Int., 41 (2015) 2806.
13. M.-C. Huang, T. Wang, C.-C. Wu, W.-S. Chang, J.-C. Lin, T.-H. Yen, Ceram. Int., 40 (2014) 10537.
14. A. Ali, H. Zafar, M. Zia, I. ul Haq, A. R. Phull, J.S. Ali, A. Hussain, Nanotechnol. Sci. Appl., 9 (2016) 49.
15. J.-M. Tulliani, C. Baroni, C. Lopez, L. Dessemond, J. Eur. Ceram. Soc., 31 (2011) 2357.
16. J. Balbuena, M. Cruz-Yusta, A. L. Cuevas, F. Martín, A. Pastor, R. Romero, L. Sánchez, J. Alloys Compd., 797 (2019) 166.

_____

17. A. K. Ramasami, T. N. Ravishankar, K. Sureshkumar, M. V Reddy, B.V.R. Chowdari, T. Ramakrishnappa, G. R. Balakrishna, J. Alloys Compd., 671 (2016) 552.

18. C. Wang, X. Cheng, X. Zhou, P. Sun, X. Hu, K. Shimanoe, G. Lu, N. Yamazoe, ACS Appl. Mater. Interfaces., 6 (2014) 12031.

19. N. Z. Tomić, M. M. Vuksanović, Đ. Veljović, V. Đokić, A. D. Marinković, R. Jančić Heinemann, Sci. Sinter., 51 (2019) 265.

20. D. Nikolić, M. Panjan, G.R. Blake, M. Tadić, J. Eur. Ceram. Soc., 35 (2015) 3843.

21. M. Airimioaei, V.A. Lukacs, I. Lisiecki, P. Beaunier, J. Blanchard, D. Lutic, S. Tascu, P. Postolache, C.E. Ciomaga, M. Olariu, L. Mitoseriu, J. Alloys Compd., 816 (2020) 152543.

22. S. Hadke, M.T. Kalimila, S. Rathkanthiwar, S. Gour, R. Sonkusare, A. Ballal, Ceram. Int., 41 (2015) 14949.

23. G. Turgut, E. Sonmez, S. Duman, Ceram. Int., 41 (2015) 2976.

24. M. Vanags, A. Šutka, J. Kleperis, P. Shipkovs, Ceram. Int., 41 (2015) 9024.

25. E. A. Gibson, M. Awais, D. Dini, D. P. Dowling, M. T. Pryce, J. G. Vos, G. Boschloo, A. Hagfeldt, Phys. Chem. Chem. Phys., 15 (2013) 2411.

26. T. C. Ooi, S. Campbell-Hardwick, D. Zhu, J. Pan, Miner. Process. Extr. Metall. Rev., 35 (2014) 266.

27. R. Sepúlveda, A. A. Plunk, D. C. Dunand, Mater. Lett., 142 (2015) 56.

28. J. Tong, D. Clark, M. Hoban, R. O'Hayre, Solid State Ionics., 181 (2010) 496.

29. S. Filipović, N. Obradović, S. Marković, A. Đorđević, I. Balać, A. Dapčević, J. Rogan, V. Pavlović, Sci. Sinter., 50, 4 (2018) 409.

30. G. S. Upadhyaya, Sci. Sinter., 50 (2018) 501.

31. J. Šubrt, L.A. Pérez-Maqueda, J. M. Criado, C. Real, J. Boháček, E. Večerníková, J. Am. Ceram. Soc., 83 (2000) 294.

32. M. Imran Din, A. Rani, Int. J. Anal. Chem., 2016 (2016).

33. S.-B. Wang, Y.-L. Min, S.-H. Yu, J. Phys. Chem. C., 111 (2007) 3551.

34. D. Mateos, B. Valdez, J. R. Castillo, N. Nedev, M. Curiel, O. Perez, A. Arias, H. Tiznado, Ceram. Int., 45 (2019) 11403.

35. M. B. Ponnuchamy, G. M. Muralikrishna, V. R. Mannava, G. S. Reddy, Ceram. Int., 44 (2018) 15019.

36. M. Farbod, V. K. Dehbidi, M. Z. Shoushtari, Ceram. Int., 43 (2017) 13670.

37. S. P. Jahromi, N. M. Huang, M. R. Muhamad, H. N. Lim, Ceram. Int., 39 (2013) 3909.

38. T. A. Lastovina, A. P. Budnyk, M. A. Soldatov, Y. V Rusalev, A. A. Guda, A. S. Bogdan, A. V Soldatov, Mendeleev Commun., 27 (2017) 487.

39. M. Tadic, D. Trpkov, L. Kopanja, S. Vojnovic, M. Panjan, J. Alloys Compd., 792 (2019) 599.

40. Z. Fereshteh, M. Salavati-Niasari, Adv. Colloid Interface Sci., 243 (2017) 86.

41. A. R. García, A. G. Laverat, C. V. R. Prudencio, A. J. Méndez, Thermochim. Acta., 213 (1993) 199.

42. Z.-L. Sun, J. Therm. Anal. Calorim., 79 (2005) 731.

43. D. Dollimore, J. Pearce, J. Therm. Anal., 6 (1974) 321.

44. N. Kumar, P.L. Kachroo, R. Kant, J. Therm. Anal., 17 (1979) 81.

45. L. Odochian, A.M. Mocanu, C. Moldoveanu, G. Carja, C. Oniscu, J. Therm. Anal.

_____

Calorim., 94 (2008) 329.

46. J. C. De Jesus, I. González, A. Quevedo, T. Puerta, J. Mol. Catal. A Chem., 228 (2005) 283.

47. M. Iacob, C. Racles, C. Tugui, G. Stiubianu, A. Bele, L. Sacarescu, D. Timpu, M. Cazacu, Beilstein J. Nanotechnol., 7 (2016) 2074.

48. M. Kamruddin, P. K. Ajikumar, N. R., A. K. Tyagi, B. Raj, Scr. Mater., 50 (2004) 417.

49. D. A. Jeremić, G. N. Kaluđerović, S. Gómez-Ruiz, I. Brčeski, B. Kasalica, V. M. Leovac, Cryst. Growth Des., 10 (2010) 559.

50. W. Henderson, B. K. Nicholson, Acta Crystallogr. Sect. C., 51 (1995) 37.

51. R. W. Cheary, A. Coelho, J. Appl. Crystallogr., 25 (1992) 109.

52. N. Dharmaraj, P. Prabu, S. Nagarajan, C. H. Kim, J. H. Park, H. Y. Kim, Mater. Sci. Eng. B., 128 (2006) 111.

53. F. Davar, H. Hadadzadeh, T. S. Alaedini, Ceram. Int., 42 (2016) 19336.

54. M. Mohammadikish, Ceram. Int., 40 (2014) 1351.

Сажетак: У овом раду је први пут дата веома једноставна и брза синтеза наночестица никл-оксида (NiO) и хематита (α-Fe₂O₃) изведена у једном кораку термалном декомпозицијом аква комплекса прелазних метала чији је анјон камфор сулфонат. Добијени нано прахови су окарактерисани рендгенском дифракцијом на праху, ИЦ спектроскопијом, скенирајућом електронском микроскопијом и енергијски дисперзивном рендгенском спектроскопијом. Рендгенска дифракција на праху потврдила је формирање NiO и α-Fe₂O₃ кристалних фаза велике чистоће. Просечне димензије кристалита α-Fe₂O₃ су биле око пет пута веће у односу на кристалите NiO. ИЦ спектри синтетисаних материјала показују карактеристичне траке за наноструктуре NiO и α-Fe₂O₃. За визуелизацију морфологије и одређивање хемијског састава финалних производа коришћене су скенирајућа електронска микроскопија и енергијски дисперзивна рендгенска спектроскопија. Термогравиметријска анализа је омогућила боље разумевање термичког понашања прекурсора. Ова брза и лако изводљива метода синтезе отвара широк спектар примене добијених материјала, нарочито због своје економске исплативости.
Кључне речи: наноматеријали, никл-оксид, хематит, камфор сулфонати, синтеза у једном кораку.